Near- and long-term quantum algorithmic approaches for vibrational spectroscopy

Nicolas P. D. Sawaya, Francesco Paesani, and Daniel P. Tabor

Near- and long-term quantum algorithmic approaches for vibrational spectroscopy

Nicolas P. D. Sawaya,[1, *] Francesco Paesani,[2, 3, 4] and Daniel P. Tabor[5, †]

[1]*Intel Labs, Santa Clara, CA 95054, USA*

[2]*Department of Chemistry and Biochemistry,*

University of California San Diego, La Jolla, CA 92093, USA

[3]*Materials Science and Engineering,*

University of California San Diego, La Jolla, CA 92093, USA

[4]*San Diego Supercomputer Center, University of*

California San Diego, La Jolla, CA 92093, USA

[5]*Department of Chemistry, Texas A&M University, College Station, TX 77843, USA*

Abstract

Determining the vibrational structure of a molecule is central to fundamental applications in several areas, from atmospheric science to catalysis, fuel combustion modeling, biochemical imaging, and astrochemistry. However, when significant anharmonicity and mode coupling are present, the problem is classically intractable for a molecule of just a few atoms. Here, we outline a set of quantum algorithms for solving the molecular vibrational structure problem for both near- and long-term quantum computers. There are previously unaddressed characteristics of this problem which require approaches distinct from most instances of the commonly studied quantum simulation of electronic structure: many eigenstates are often desired, states of interest are often far from the ground state (requiring methods for "zooming in" to some energy window), particle conservation is not required, and transition amplitudes with respect to a non-unitary Hermitian operator must be calculated. We address each of these hurdles and consider problem instances of four molecular vibrational Hamiltonians. Finally and most importantly, we give analytical and numerical results which suggest that, to a given energy precision, a vibrational problem instance will be simulatable on a quantum computer before an electronic structure problem instance. These results imply that more focus in the quantum information community ought to shift toward scientifically and industrially important quantum vibrational problems.

---

* nicolas.sawaya@intel.com

† daniel_tabor@tamu.edu

I. INTRODUCTION

To date, the vast majority of chemistry- and materials-related quantum algorithms research has focused on the electronic structure (ES) problem [1, 2]. Given a particular set of nuclear coordinates, the goal is to solve the time-independent fermionic (electronic) many-body problem to determine accurate energies. However, an accurate solution of the ES problem is only one of the current challenges in computational chemistry and materials science. There are properties of interest for which the computational bottleneck is not ES, but rather an accurate quantum treatment of the molecular motion [3].

One such area is the simulation of vibrational structure (VS) and determination of vibrational spectra, as there is a large subset of molecules for which ES *is* classically tractable to subchemical accuracy while the quantum vibrational problem is not (see Figure 1). This is true for small molecules and clusters [4–8] in several areas of spectroscopy: infrared spectra, Raman spectra, vibronic spectra, and ultrafast vibrational spectra, to name just a few [9–11].

Even qualitatively correct vibrational spectra often require a rigorous quantum treatment because Fermi resonances, association bands, and other resonance effects can result from small coupling terms [9, 13–15]. The ability to simulate vibrational structure has many applications including fuel combustion [16], atmospheric science [17], astrochemistry [18, 19], and fundamental experiments in chemical physics [20, 21]. Other than vibrational spectra, problems that lie in the lower-left quadrant of Figure 1 include low-temperature thermodynamic calculations of some bulk solids [22] and quantum liquids [23].

Previous quantum computational studies in this area include analog quantum algorithms for quantum vibrations [24–28], digital quantum algorithms for finding vibrational states and/or overlaps [3, 29, 30], and approaches for which vibrational degrees of freedom are coupled to other systems [31–34]. The present work is distinct in that we outline the several conceptual peculiarities of simulating vibrational spectroscopy, we apply quantum algorithms that had not previously been used in this context, and we study the complexity of VS relative to ES.

In this work we present algorithms for calculating vibrational spectra on both near- and long-term hardware, focusing on vibrational infrared spectra. One of our contributions is identifying certain essential components that are required for this problem class, drawing
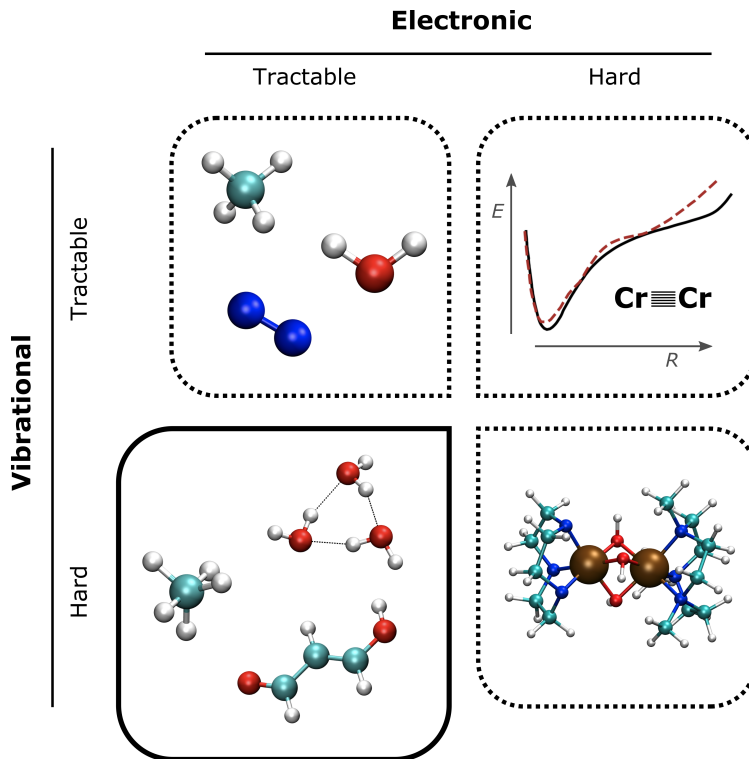
FIG. 1. We categorize molecular simulation into four quadrants, depending on whether the electronic structure and vibrational structure of the problem are tractable on a classical computer. This work's focus is the lower-left quadrant—those molecules or complexes for which the potential energy surface can be calculated on a modern classical computer, while the quantum vibrational structure may require a quantum computer. *Upper-left*: small rigid molecules methane, water, and nitrogen. *Upper-right*: the chromium dimer (dashed: calculation; solid: experiment) [12]. *Lower-right*: A chromium-containing large molecule with non-rigid ligands. *Lower-left*: the prototypical "fluxional" molecule CH_5^+, the water trimer, and malondialdehyde.

attention to the algorithmic objectives that would not appear in most other common problems that involve Hamiltonian simulation. Some aims of this class of problems, which we introduce to the reader and demonstrate how to address, are significantly different from ES. Finally and most importantly, we compare the problem's complexity characteristics to ES. The results lead us to cautiously predict that, for a given precision, a VS problem instance will probably achieve quantum advantage before an ES one.

From a Hamiltonian simulation perspective, we note five conceptual differences between the nature of the typical ES problem instance and that of vibrational spectroscopy, the first

3

three of which to our knowledge have not been clearly stated previously in this context. First, when it is said that the "spectrum" is being calculated in molecular ES, this normally refers to only a few of the lowest-lying electronic states. In contrast, in a vibrational problem one is almost always interested in many states. Second, the states of interest are often far (in quanta) from the ground state—excited states above the 100th energy level are often of interest.

The third conceptual difference is that one is often interested in calculating both vibrational energies and transition intensities, which necessitates calculating the transition amplitudes with respect to a non-unitary coordinate-dependent operator. Though such transition amplitudes are applicable to ES in some important areas [35, 36], their inclusion has not been the norm in the context of quantum algorithms. Fourth, the problem requires that vibrations (bosons) instead of fermions be encoded into the quantum device, a topic that has been previously explored [3, 37–39]. Finally, particle conservation [40, 41] is not a factor in vibrational spectroscopy, which may lead to simpler algorithm components.

II. THEORY

In arbitrary internal coordinates $\vec{s}$ (with corresponding momenta $\vec{m}$), the Hamiltonian for M vibrations in general form is written (with $\hbar = 1$) $H = \frac{1}{2} \sum g_{ij} m_i m_j + V(\vec{s})$ where g_{ij} is the coupling between momenta (vanishing for $i \neq j$ under normal or Cartesian coordinates) and $V(\vec{s})$ is the potential energy term. In the harmonic approximation, one may diagonalize the Hessian matrix at the equilibrium position, leading to a simplified approximate expression with uncoupled coordinates, $H_{\text{harm}} = \frac{1}{2} \sum_i^M \omega_i (q_i^2 + p_i^2)$, where i denotes the vibrational mode, M is the total number of modes, q and p are respectively the bosonic position and momentum operators, and ω_i is the energy of mode i. It is trivial to find eigenvalue-eigenfunction pairs for the harmonic Hamiltonian on a classical computer, since excited states in the Harmonic approximation are product states of separate modes.

The harmonic Hamiltonian can be systematically improved by including higher order anharmonic terms,

$$H_{\text{anharm}} = \frac{1}{2} \sum_i^M \omega_i (q_i^2 + p_i^2) + \sum_{\{ijk\}} h_{ijk} q_i q_j q_k + \sum_{\{ijkl\}} h_{ijkl} q_i q_j q_k q_l + \cdots, \qquad (1)$$

where the index ordering is irrelevant and $h_{ijk\cdots} = 0$ if all indices are distinct. Computational

difficulties arise when these higher-order terms are included, due to both the deviation from harmonicity and the coupling between modes.

Even for a molecule of 5 to 8 atoms, the complete inclusion of anharmonic effects can be computationally prohibitive. Though various forms of perturbation theory and dimensionality reduction sometimes yield good results, one must often resort to exact diagonalization of the whole Hilbert space (which scales exponentially in the number of modes) or similarly expensive methods [42–47]. In any molecule whose vibrational Hilbert space is too large for a classical computer and which also requires exact diagonalization, one would likely require the use of a quantum computer. Note we are not constrained to use the harmonic basis of equation (1)—it will often be the case that choosing a specialized coordinate system allows one to use a lower-order series expansion [30, 48–50].

In order to make our discussion concrete, we consider infrared spectroscopy, though similar mathematical methods would be used for other experiments such as Raman, microwave, or ultrafast multidimensional vibrational spectroscopy [9, 10]. The dipole moment operator is necessary for simulation of light-matter interaction, $e.g.$ for calculating transition intensities. It is denoted $\mu^{(\alpha)}$ where $\alpha \in \{x, y, z\}$ is a Cartesian direction, and may also be expanded in a power series,

$$
\begin{aligned}
\mu^{(\alpha)} &= \mu_0^{(\alpha)} + \sum_i^M \left. \frac{\partial \mu^{(\alpha)}}{q_i} \right|_{q_i=0} q_i + \frac{1}{2} \sum_{ij}^M \left. \frac{\partial^2 \mu^{(\alpha)}}{q_i q_j} \right|_{q_i, q_j=0} q_i q_j + \cdots \\
&= \mu_0^{(\alpha)} + \sum_i^M m_i q_i + \sum_{ij}^M m_{ij} q_i q_j + \cdots
\end{aligned}
\tag{2}
$$

The objective is to calculate the spectrum

$$
f(\omega) = \sum_\alpha \sum_j |\langle 0 | \mu^{(\alpha)} | j \rangle|^2 \mathcal{L}(\omega_j - \omega),
\tag{3}
$$

where $|0\rangle$ is the initial eigenstate (ground state when beginning from zero temperature), and $\mathcal{L}(\omega)$ is a line shape function, approximated as a delta function when one does not consider broadening effects. Though in this work we consider transitions from the ground state, the initial state of interest is often a Gibbs state ($i.e.$ thermal state). Existing quantum algorithms for thermal state preparation [51–55] may be used in conjunction with the approaches summarized here.

Both the Hamiltonian and the dipole operator may be mapped to a qubit-based Hamiltonian using the bosonic commutation relations, where a practical choice is to use the

Pauli operator basis: $H_{\text{anharm}} \mapsto \sum_k^{N_P} a_k P_k = \sum_k a_k \bigotimes_g^{N_q} \sigma_{gk}$ and $\mu^{(\alpha)} \mapsto \sum_k^{N_R^{(\alpha)}} b_{k\alpha} R_{k\alpha} = \sum_k b_{k\alpha} \bigotimes_g^{N_q} \sigma_{gk\alpha}$, where g labels the qubit, $\sigma \in \{I, X, Y, Z\}$ is the identity or a Pauli operator, α labels the Cartesian direction, N_P (N_R) is the number of Pauli strings in the encoded Hamiltonian (dipole operator), and N_q is the number of qubits. Approaches for performing this mapping have been discussed previously [3, 31, 37, 38].

A near-term algorithm for the vibrational spectroscopy problem requires several elements: (a) mapping of bosons to qubits, (b) finding unitaries U_i to produce eigenstates, (c) determining state overlaps $|\langle \psi_i | \psi_j \rangle|^2$, (d) calculating transition amplitudes with respect to a non-unitary Hermitian operator, and (e) efficiently finding eigenstates far above the ground state. We first present the noisy intermediate-scale quantum (NISQ) approach for these problem requirements in Sections II A and II B, then provide commentary and approaches regarding partial spectra in Sections II C and II D, before briefly summarizing a long-term approach that addresses all algorithmic requirements in Section II E.

A. Eigenfunction finding on near-term hardware

In this Section we briefly summarize existing NISQ methods for finding eigenvalues; more importantly, we elaborate on three of the essential ways in which the simulation of vibrational spectroscopy is conceptually different from problems in ES.

Using near-term quantum hardware, ground and excited states may be found by using previously published variational methods [40, 53, 56–59]. For a given vibrational eigenstate $|\psi_j\rangle$, a variational method used with a classical optimizer will lead to a circuit unitary U_j yielding $U_j|0\rangle = |\psi_j\rangle$. This stored circuit U_i is then used to find transition amplitudes, as described below.

An important characteristic of this problem is that (unlike in ES) there is no need for particle conservation. Any state $|\psi\rangle$ produced by an arbitrary (even error-prone) quantum circuit is valid. This may imply that such problems can be solved in shorter depth than particle-conserving problems like ES or the Bose-Hubbard model [32], since (a) one has more freedom in choosing a quantum ansatz and (b) hardware errors will never lead to deviations from the manifold of valid states (since the whole manifold is valid).

The second difference between VS and ES to reiterate is that one is often interested in many vibrational states in one energy region, as opposed to just a few in ES. Sometimes even

a somewhat coarse-grained spectrum is sufficient for vibrational spectroscopy applications. This is discussed further in Section II E. The third distinction is that in VS one is often interested in very high-lying states, including the 100th excited state or higher, as discussed in Section II C. Most of the standard NISQ methods for finding eigenvalues cited above are not efficient for overcoming these two hurdles, highlighting these areas as fruitful for new research.

B. Near-term algorithms for transition amplitudes

Before discussing a method for calculating arbitrary transition amplitudes, we give two known methods for calculating $|\langle \eta_i | \eta_j \rangle|^2$, an important primitive. In the first method, one implements $U_i^\dagger U_j$. Thereafter, the fraction of measurements that equal the all-zero vector $|0\rangle^{\otimes N_q}$ is equal to the overlap squared [60]. This method does not require additional qubits, though the final circuit depth is equal to the sum of the two unitaries' depths. The second method is to use a SWAP test [61] or destructive SWAP test [62], which doubles the number of qubits but increases the depth only by a small constant factor.

In order to calculate arbitrary transition amplitudes $|\langle \psi_i | A | \psi_j \rangle|^2$ on near-term hardware, a naive approach would require a method for considering cross-terms in addition to their absolute values squared. This is a nontrivial task, since quantum computers naturally output overlaps squared. Though inner products may be calculated with so-called Hadamard tests that require a substantially increased circuit depth if only one- and two-qubit gates are allowed [63], Ibe et al. recently found a much shorter-depth method [64] for calculating transition amplitudes of arbitrary operators.

Tailoring the latter work to vibrational spectroscopy, one may use an additional set of unitaries, $V_{kl,\pm}^{(\alpha)} = \frac{1}{2}(I \pm iR_{k\alpha})(I \pm iR_{l\alpha}) = e^{\pm iR_{k\alpha}\pi/4}e^{\pm iR_{l\alpha}\pi/4}$, for all $l, k < N_R^{(\alpha)}$, where $N_R^{(\alpha)}$ is the number of Pauli terms in $\mu^{(\alpha)}$. One then proceeds to reproduce $|\langle i | \mu^{(\alpha)} | j \rangle|^2$ from many measurements on the circuit set $U_i^\dagger V_{kl,\pm} U_j |0\rangle$. Thus one increases the depth of two state preparation circuits by a small constant factor and collects measurement statistics from many different circuits. This procedure is performed on every eigenstate for which one wishes to calculate the transition amplitude. The fact that this algorithm increases circuit depth by only a small factor makes it ideal for near-term hardware.

The full expression for the transition amplitudes is

$$|\langle i|\mu^{(\alpha)}|j\rangle|^2 = \sum_k b_{k\alpha}^2 |\langle i|R_{k\alpha}|j\rangle|^2$$

$$+ \sum_{k<l} b_{k\alpha} b_{l\alpha} \left[2|\langle i|V_{kl,+}^{(\alpha)}|j\rangle|^2 + 2|\langle i|V_{ij,-}^{(\alpha)}|j\rangle|^2 - |\langle i|R_{k\alpha}|j\rangle|^2 - |\langle i|R_{l\alpha}|j\rangle|^2 - |\langle i|R_{l\alpha}R_{k\alpha}|j\rangle|^2 \right].$$

$$(4)$$

Terms such as $|\langle i|R_{k\alpha}|j\rangle|^2$ are determined by preparing state $U_i^\dagger \exp(i\frac{\pi}{2}R_{k\alpha})U_j|0\rangle$ before counting zero strings. Expressions $\exp(\pm i\theta R_{k\alpha})$ can be implemented in short depth using well known primitives [65]. The number of required circuits scales quadratically with the number of Pauli strings $N_R^{(\alpha)}$ in the dipole operator.

The advantage of Ibe et al.'s approach is that Hadamard tests [63] are not needed; Hadamard tests would require controlled-U_i unitaries. Assuming the quantum hardware uses one- and two-qubit gates, this would require each three-qubit gate to be decomposed into many one- and two-qubit gates [65], considerably increasing the circuit depth. However, this reduction in circuit depth comes at the cost of requiring a larger number of measurements.

Some comments on hardware noise is merited. The effect of noise and other errors on near-term quantum algorithms has been studied in the context of quantum chemistry [40, 66, 67], and methods have been developed for partially mitigating such errors [68–70]. We do not study noise in this work, partly because we find it unlikely that the inclusion of noise would affect VS and ES differently enough to eliminate the large numerical difference observed in Section IV A. However, we note that the most important heuristic for dealing with noise in near-term hardware is to use shorter circuit depths, as this allows less time for decoherence to reduce fidelity. Hence in near-term hardware it will usually be worth trading a reduction in circuit depth for an increase in another resource, *e.g.* the above-mentioned increase in the number of required measurements.

C. Spectral window focusing

Not only are we often interested in many vibrational eigenstates—it is also often the case that one is concerned *only* with high-lying excited states (for instance the 100th excited state and above). This may be the case when: part of a spectrum is blocked by background noise; an astronomical telescope is able to read only part of the infrared spectrum; or only

a specific band is technologically relevant. Therefore it may be a waste of computational effort to find eigenstates outside the energy window of interest.

We point this out because it means the *goal* of the vibrational spectrum problem often differs from other Hamiltonian simulation problems, leading to important considerations in algorithm design that have not been widely investigated.

The notable consequence is that most hereto proposed near-term algorithms for excited states are not always viable. This is because in their canonical forms, most existing near-term approaches [53, 56, 57, 59, 71, 72] require one to find the low-energy eigenvector subspace as a way to build up to the desired excited state.

We highlight one possible (previously proposed) near-term algorithmic solution for determining high-lying excited states, that may be used in conjunction with the previously mentioned methods. This is to use the folded spectrum method [40, 58], which easily allows one to select any energy neighborhood. The folder Hamiltonian is defined as

$$H_{fold} = (H - \zeta I)^2 \tag{5}$$

where ζ is an arbitrary constant. The lowest eigenstates of H_{fold} are those eigenstates of H which are closest in energy to ζ. This approach quadratically increases the number of Pauli terms in the effective Hamiltonian, allowing one to "zoom in" on an arbitrary portion of the spectrum. We do not rule out more efficient near-term methods for high-lying excited states.

D. The utility of incomplete vibrational spectra

When using variational algorithms and NISQ hardware to determine portions of the spectra, one may be able to calculate only incomplete spectra. This is due to the nature of many hybrid quantum-classical algorithms; it is usually not possible to guarantee that all eigenstates in a given energy region have been found. Hence it is important to note that even a spectrum with missing peaks is often useful. First, one may be interested in only a few specific spectral features in the region, in which case one may focus efforts converging to those specific transitions. Second, and perhaps more importantly, the goal is often to determine whether a candidate molecule matches an experimental result. If some spectral features in the computed spectrum of the candidate molecule are not present in the

experimental spectrum, then the candidate molecule may be removed from consideration.

E. Long-term approaches

In the more typical use of QPE, one first attempts to prepare a state with as much overlap as possible with a particular eigenstate, *e.g.* the ground state. In the context of this work, QPE is used differently, in a way that allows one to calculate a full response spectrum [29, 73, 74], *i.e.* determining $|\langle \eta_0 | \hat{A} | \psi_i \rangle|^2$, where $\hat{A} | \eta_0 \rangle$ is generally not an eigenstate of the Hamiltonian but the $\{|\psi_i\rangle\}$ are eigenstates. First consider the case of $\hat{A} = \hat{I}$. One runs the same QPE algorithm, but sets the initial state to $|\eta_0\rangle$ (in general not an eigenstate) such that $|\eta_0\rangle = \sum_i c_i |\psi_i\rangle$. After running QPE, one is left with a superposition of eigenstate-eigenphase pairs, as shown in the expression

$$\sum c_i |\psi_i\rangle |0\rangle \xrightarrow{\text{QPE}} \sum c_i |\psi_i\rangle |\tilde{\phi}_i\rangle. \tag{6}$$

In contrast to the standard use of QPE, in this case we are interested in more than just one eigenstate. The algorithm proceeds as follows. The state is stored in register S and the eigenphase in register E. One performs many repetitions of the circuit, measuring register E after each run, yielding a phase $\tilde{\phi}_i$. From many measurements one then composes a histogram where each bin is an N_E-bit value $\tilde{\phi}_i$. This histogram is the desired response spectrum with resolution determined by N_E, and the process terminates once the histogram has converged.

One advantage of this method is that it combines many eigenstates into a single measurement, effectively coarse-graining the eigenstates to a desired precision (Section II A) [29, 73, 74]. This is especially useful for vibrational spectroscopy, where it is often acceptable to combine the intensities of many eigenstates in a narrow energy range. For a particular N_E, there is a subset of eigenstates $\mathcal{D}_j = \{\psi_{j1}, \psi_{j2} \cdots\}$ all of which yield $\tilde{\phi}_j$. Hence if the measurement yields $\tilde{\phi}_j$, this means register S has collapsed to the superposition $\mathcal{N} \sum_{k \in \mathcal{D}_j} c_k |\psi_k\rangle$, where $\mathcal{N}$ is a normalization constant. The beneficial result is that the probabilities of many nearby eigenenergies are combined, and the number of required measurements is dependent on N_E but *independent* of the size of the problem Hamiltonian.

As discussed, vibrational (*e.g.* infrared) spectroscopy requires calculating the action of an arbitrary non-unitary operator $\mu^{(\alpha)}$ on a prepared state. Roggero *et al.* [74] solved the

problem of linear response with respect to a non-unitary operator. We adapt their method here. After adding one ancilla qubit, one may apply the operator

$$U_{\mu,\alpha,\gamma} = \begin{pmatrix} \cos\gamma\mu^{(\alpha)} & -\sin\gamma\mu^{(\alpha)} \\ \sin\gamma\mu^{(\alpha)} & \cos\gamma\mu^{(\alpha)} \end{pmatrix} \tag{7}$$

to an arbitrary state $|\psi\rangle$, which will yield $\mathcal{N}\mu^{(\alpha)}|\psi\rangle$ with probability $P_{success} = \langle\psi|\sin(\gamma\mu^{(\alpha)})|\psi\rangle$, where $\mathcal{N} = ||\mu^{(\alpha)}|\psi\rangle||^{-1}$ is a normalization constant. This unitary probabilistically produces the desired state $|\Phi_0^{(\alpha)}\rangle \equiv \hat{\mu}^{(\alpha)}|\eta_0\rangle/||\hat{\mu}^{(\alpha)}|\eta_0\rangle||$. If the ancilla is measured to be $|0\rangle$ then the state preparation has succeeded; a $|1\rangle$ measurement indicates failure and the procedure is repeated. The remainder of the algorithm then proceeds as in the $\hat{A} = \hat{I}$ case, with $|\eta_0\rangle$ replaced by $|\Phi_0^{(\alpha)}\rangle$.

Finally, we posit that there are promising strategies for "spectral window focusing" in long-term hardware as well. For the QPE-based method, the goal would be to make the histogram measurements fall primarily within a particular energy window, as measurements outside the window are not of interest. In principle one may use amplitude amplification methods [75, 76] to boost the probability of the desired eigenenergy window. The result is that fewer measurements would be required to produce the histogram in the energy window of interest, at the cost of an increase in circuit depth. We leave a full description to future work.

III.   COMPARISON TO ELECTRONIC STRUCTURE PROBLEMS

The first physics simulation to achieve quantum advantage is likely to be a nearest-neighbor toy model such as an Ising model [77], because only $\mathcal{O}(N)$ two-body interactions are present. But it is important to consider what will be the first real-world non-toy simulation to show quantum advantage. Here we argue that, to a given energy precision, the first such simulation of a molecule is more likely to be a vibrational problem instance than an electronic one. The ES Hamiltonian may be written as $H_{\mathrm{ES}} = \sum h_{ij} a_i^\dagger a_j + \sum h_{ijkl} a_i^\dagger a_j^\dagger a_k a_l$ where $a_i^\dagger$ and a_i are fermionic creation/annihilation operators for the ith orbital. In real molecules one effectively observes nearly all-to-all connectivity between the electronic orbitals (see SI).

The quantum resources required for the vibrational problem depend on the order of the expansion needed for sufficient precision in equation (1). We observe that early molecular

targets for quantum computing ought to be those for which (a) classical computational approaches (*e.g.* perturbation theory) fail and (b) sufficient accuracy can be achieved by including at most three-body terms. Both requirements are likely to hold for a substantial set of molecules [78, 79].

A third-order vibrational Hamiltonian in normal coordinates has four types of terms: p_i^2, q_i^2, q_i^3, $q_i^2 q_j$. A fourth-order Hamiltonian has eight types, with the inclusion of q_i^4, $q_i^3 q_j$, $q_i^2 q_j^2$, and $q_i^2 q_j q_k$. A key insight is that vibrational Hamiltonians that include at most three-body terms will scale at most as $\mathcal{O}(M^3)$ in the number of modes M. However, depending on the choice of coordinate system [48–50, 79] it is often possible to exclude three-body interactions, leading to a scaling of $\mathcal{O}(M^2)$ terms. This scaling is more favorable than molecular ES, for which near-term implementations would require approximately $\mathcal{O}(N^4)$ Hamiltonian terms in the number of orbitals N. Notably, it is more common to see sparser interactions in VS problems than in ES problems.

Our case hinges on the notion that a Hamiltonian with more terms and with higher Pauli lengths is likely to require more resources to simulate, regardless of whether one is using near- or long-term hardware. (The Pauli length of a string is the number of single-qubit terms it contains; *e.g.* $X_0 X_3 Z_5$ has a Pauli length of 3.) However, the asymptotic scaling on its own does not provide enough evidence. One must still investigate (a) whether the pre-factor to the vibrational Hamiltonians' term count is sufficiently small for lower qubit counts, (b) the locality of the Hamiltonians, and (c) Hamiltonian magnitudes, all of which we study below.

An essential comment is merited regarding the direct comparison between these two problem classes. For the comparison between vibrational and electronic problems, the appropriate independent variable is indeed the number of qubits (not the number of electron orbitals or vibrational modes). This is because most of the earliest problem instances for which one would need a quantum computer are likely to be those for which exact diagonalization is required (because we are assuming that even methods such as perturbation theory fail). Hence to compare different problem types it is appropriate to make direct comparisons only between two problem instances with *similarly sized Hilbert spaces*, which is the same as saying similar qubit counts. And as a practical matter, available quantum hardware will have a given qubit count and maximum circuit depth, and the question at hand would be whether that given hardware would be able to perform some classically intractable problem
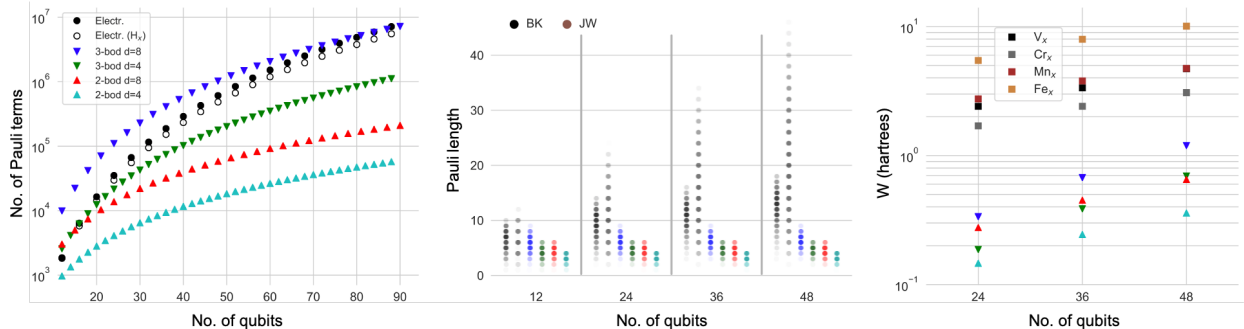
FIG. 2. *Left:* Number of Pauli strings in each Hamiltonian class. Circles denote electronic structure Hamiltonians; triangles denote analytical results for fourth-order vibrational Hamiltonians. In the case of electronic structure, the number of qubits is equal to twice the number of spatial orbitals, while in vibrational structure the number of qubits is equal to $\log_2 d$ times the number of modes. *Center:* Probability distributions of Pauli lengths in six Hamiltonian classes. BK and JW respectively denote the Bravyi-Kitaev and Jordan-Wigner mappings. *Right:* The Hamiltonian magnitude W, which should be compared only between Hamiltonians with Hilbert spaces of the same size.

instance.

Notably, there has been considerable recent progress in reducing the asymptotic scaling of quantum algorithms for ES [80–83]. However, due to these newer algorithms' need for a larger basis set and/or an increase in the number of required qubits, these methods are unlikely to be amenable to accurate molecular simulation for qubit counts below 1000 [83]. Further, even if one assumes that error-corrected hardware is required for solving *any* instance of both the vibrational and electronic problems, it appears likely that the subset of vibrational problems with $\mathcal{O}(M^2)$ or $\mathcal{O}(M^3)$ Pauli terms will be solvable before any ES instance, based on our analysis. SI Section S5 include extensive additional discussion.

IV. RESULTS

A. Proxies for quantum resource comparisons

All our vibrational data is for fourth-order Hamiltonians, where we use bosonic truncations $d = 4$ or 8 and have considered both the exclusion and inclusion of 3-body terms $q_i^2 q_j q_k$.

The left panel of Figure 2 shows the number of terms in various ES and VS Hamiltonians, plotted against qubit count. For the majority of cases considered here, these results show that the ES Hamiltonians contain more terms for qubit counts great than $\sim$20.

For simplicity, we consider only cases in which all modes have equal d. In reality, each mode would require a different truncation, meaning that the number of Pauli strings would lie in between the plotted trends. For the electronic problem instances, the analytical results (filled circles) are comparable to the numerical results (open circles) obtained from 3D grids of hydrogen atoms (see SI). Note that the number of Pauli terms is equal for the Jordan-Wigner (JW) [84] and Bravyi-Kitaev (BK) [85] encodings, though their length distributions are unequal.

The center panel of Figure 2 shows the distribution of Pauli lengths, another important indicator of a problem Hamiltonian's simulation complexity. For the subset of vibrational problem instances considered (fourth-order Hamiltonians with truncations of $d \leq 8$), vibrational problems are more local than electronic problems, even for low qubit counts and when compared against the logarithmically scaling BK mapping.

A third factor determining simulation complexity is the magnitude of the Hamiltonian. There are different matrix norms used in quantum algorithm analysis, and resource bounds are usually derived in terms of both a norm and the desired precision, among other considerations [77, 86–89]. In addition, the number of measurements for VQE depends on the magnitude of the terms [40, 90], which is closely related to our expression below. For a simple and easily computed comparison of Hamiltonian magnitudes, we use the quantity $W = \sqrt{\sum_{k \neq k_I} a_k^2}$ where $k \neq k_I$ signifies that the coefficient preceding the identity operator is excluded. Notably, $W 2^{N_q/2}$ is an upper bound to the Frobenius norm. W should be used for comparisons only between Hamiltonians on the same number of qubits.

We constructed minimal-basis ES model Hamiltonians for transition metals V_x, Cr_x, Mn_x, and Fe_x, where $x = 2$, 3, and 4 correspond to 24, 36, and 48 qubits, respectively (see SI). These were meant to provide typical order-of-magnitude matrices for transition metal elements. Molecules containing these elements are likely to be the early candidates for quantum advantage in ES [91–93], especially since classical methods are already sufficiently accurate for main-group elements (*i.e.* not transition metal elements) up to a thousand orbitals [93–95]. We constructed vibrational Hamiltonians with deliberately pessimistically large couplings. Harmonic values were evenly spaced between 1000 and 4000 cm^{-1}, every

third-order vibrational term was set to 400 cm^{-1}, and every fourth-order term was set to 40 cm^{-1}.

Despite the intentionally complex vibrational Hamiltonians, W values for the two-body Hamiltonian are close to an order of magnitude smaller than the four types of electronic model Hamiltonians, while W for the three-body vibrational Hamiltonians remain several times smaller (right panel of Figure 2).

We note again that the required quantum resources are dependent on required precision, which in turn is application-dependent. A reasonable candidate for the first practical vibrational problem is the calculation of zero-point energy or low-lying transitions in a vibrational problem to sub-chemical precision (see SI Section S4). Detailed resource estimates are beyond the scope of this work, but these order-of-magnitude differences between vibrational and electronic Hamiltonians are noteworthy.

To summarize, there are four preliminary supporting pieces of evidence for our postulate that (for a given precision) quantum advantage will take place for a real-world VS problem instance before any ES problem instance:

- As mentioned in Section II A, vibrational Hamiltonians do not require particle number conservation, which may lead to less complex quantum circuits in near-term algorithms.

- There are fewer Pauli terms in the vibrational Hamiltonians, which leads to fewer operations in most quantum algorithms.

- VS Hamiltonians are more local, again leading to fewer operations and shorter circuit depths in most quantum algorithms.

- The Hamiltonian magnitude parameter W is smaller in our worst-case vibrational model than in typical-case classically difficult ES models, which implies that fewer measurements are required in near-term algorithms and that shorter circuit depths are needed in long-term algorithms.

Our argument applies *only* to the subset of vibrational problems for which at most three-body couplings are required.

B. Simulated molecular infrared spectra

As a proof of concept, we performed numerical simulations and error analyses on four vibrational Hamiltonians: carbon monoxide (CO), the isoformyl radical (COH), ozone (O_3), and a model Hamiltonian of Fermi resonance. We choose the first three molecules because they exhibit substantial anharmonicity and (for the triatomics) mode coupling, and we study the model Hamiltonian because Fermi resonances are pathological for classical methods, unless one uses a very poorly scaling algorithm such as exact diagonalization. Additionally, a conceptual reason for simulating COH is that, being a radical, it is difficult to isolate and study in the laboratory; this example highlights the need for theoretical modeling when laboratory methods fail.

In order to study parameters relevant to quantum algorithms, we calculated Suzuki-Trotter errors for both the approximate unitary used in QPE and the approximate imaginary time evolution (ITE) operator appropriate for some nearer-term algorithms. These results are specific to quantum algorithms, as Suzuki-Trotter errors based on Pauli decompositions are not relevant for classical algorithms. The results may guide the choice of time step or approximate resource counts when implementing Suzuki-Trotter decompositions in small organic molecules. For the former case, we constructed the unitary matrix

$$\tilde{U}(\Delta\tau) = \prod_{k}^{N_P} e^{-i\Delta\tau a_k P_k}. \tag{8}$$

where $\Delta\tau$ is the time step. This is a first-order Trotter approximation to the quantum propagator $U(\Delta\tau) \equiv \exp(-i\Delta\tau H)$. We then diagonalized $\tilde{U}(\Delta\tau)$ and compared the ordered eigenvalues to the exact result.

In our simulation of ITE, we instead constructed the operator

$$\tilde{M}(\Delta\beta) = \prod_{k}^{N_P} e^{-\Delta\beta a_k P_k} \tag{9}$$

where $\Delta\beta$ is an ITE step. For all but the ground state, formula (9) used the Pauli representation of the folded Hamiltonian, not of the original Hamiltonian. Folded Hamiltonians were used in order to highlight the use of a method that allows one to skip irrelevant eigenstates, effectively implementing spectral window focusing. Calculations were implemented with in-house code, using the QubitOperator class of Openfermion [96] and linear algebra routines from SciPy [97].
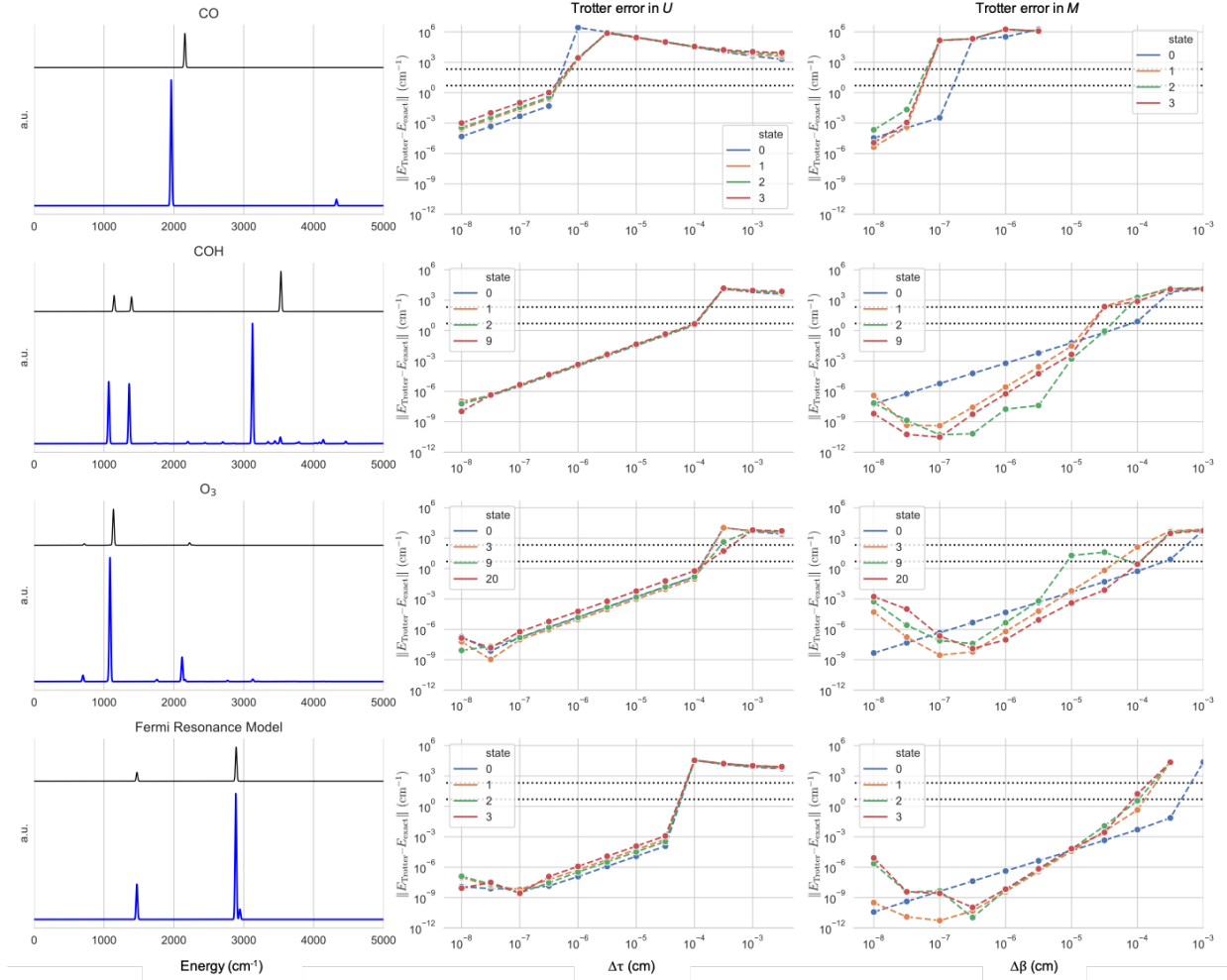
FIG. 3. Vibrational infrared spectra for carbon monoxide (CO), the isoformyl radical (COH), ozone (O_3), and a Fermi resonance model Hamiltonian. The first column shows the infrared spectra (lower blue spectra) and their harmonic approximation (upper black spectra) in arbitrary units, summing intensities in all Cartesian directions. Peaks were broadened with Gaussians of arbitrary standard deviation 10 cm^{-1}. The second column shows Trotterization error in the quantum time propagator, which is relevant to long-term algorithms. The third column shows Trotterization error in the imaginary time evolution operator, relevant to some NISQ approaches. Excited states in the third column are found using the folded Hamiltonian method. Horizontal dotted lines are drawn at 5 cm^{-1}, an arbitrary high-accuracy threshold required for many spectroscopy applications; and at 209 cm^{-1}, equal to $k_B T$ at room temperature and approximately half of chemical accuracy.

17

Figure 3 shows results for all simulated molecules. The harmonic approximations (black) are plotted with the numerically exact results (blue); the contrast between the two plots demonstrates the importance of including higher-order anharmonic terms that are hard to simulate classically. Qualitative differences such as the the extra peaks that appear (*e.g.* at 2940 cm^{-1} in the Fermi resonance Hamiltonian) tend to be difficult to obtain classically, often failing under perturbation theory [14, 79]. The second column shows the first-order Trotterization error in the quantum propagator $\tilde{U}(\Delta\tau) \approx \exp(-i\Delta\tau H)$, in a selection of intense transitions' eigenvalues against increasing $\Delta\tau$. These are related to long-term algorithms, both in running QPE and in dynamical simulations. The third column approximates the ITE operator's $\tilde{M}(\Delta\beta) \approx \exp(-\Delta\beta H)$ error by Trotterization with finite length $\Delta\beta$. These are more relevant to noisy intermediate-scale quantum (NISQ) algorithms, both for ITE [53] and variational anstazae based on ITE [98].

Errors in U are mostly independent of the eigenstates, while errors in M are distributed over many orders of magnitude even for fixed $\Delta\beta$. This may be partly because each folded Hamiltonian is in fact a different Hamiltonian. Notably, all non-monotonic behavior in the ITE error plots arise only in folded Hamiltonians—the cause of this behavior is unclear. CO requires the smallest (*i.e.* worst) time step, which we hypothesize might be due to the lack of favorable error cancellation, as cancellation may be more prominent in Hamiltonians with more terms. There was no clear trend with respect to the (Froebenius) norms of the Hamiltonians (data not shown), though in the worse case (carbon monoxide) the error becomes unacceptably large approximately when $\Delta\tau$ and $\Delta\beta$ have order of magnitude comparable to the inverse norm of the Hamiltonian ($1/\|H\|$). The resulting error trends give an indication of the step sizes needed for accurate quantum simulation of small molecules, though further study is needed to determine broadly applicable relationships between vibrational problem instances and Trotter error.

V. OUTLOOK

Although molecular electronic structure is often the first candidate offered for near-term quantum simulation of a real-world substance, we have provided evidence suggesting that molecular vibrational structure will likely, for a given energy precision, achieve quantum advantage first. After considering previously unidentified requirements in designing quan-

tum algorithms for vibrational spectra, we have presented approaches for solving this class of problems on both near-term and long-term quantum computers, addressing the components that make this mathematically distinct from more standard Hamiltonian simulation problems: calculating transition amplitudes with respect to a non-unitary operator and calculating high-lying excited states. Future research should focus on more detailed resource counts including estimates of circuit depth and gate complexity, as well as inclusion of rotational and other degrees of freedom. This work advances the applicability of quantum computation for atmospheric science, many biomolecular interactions, fuel combustion, gas-phase reactions, and astrochemistry, while implying that more focus for near-term quantum applications ought to shift to scientifically relevant vibrational problems.

[1] S. McArdle, S. Endo, A. Aspuru-Guzik, S. C. Benjamin, X. Yuan, *Rev. Mod. Phys.* **92**, 015003 (2020).

[2] Y. Cao, *et al.*, *Chem. Rev.* **119**, 10856 (2019).

[3] S. McArdle, A. Mayorov, X. Shan, S. Benjamin, X. Yuan, *Chem. Sci.* **10**, 5725 (2019).

[4] P. Jankowski, A. R. W. McKellar, K. Szalewicz, *Science* **336**, 1147 (2012).

[5] S. E. Brown, *et al.*, *J. Am. Chem. Soc.* **139**, 7082 (2017).

[6] N. Yang, C. H. Duong, P. J. Kelleher, A. B. McCoy, M. A. Johnson, *Science* **364**, 275 (2019).

[7] M. Riera, S. E. Brown, F. Paesani, *J. Phys. Chem. A* **122**, 5811 (2018).

[8] P. Bajaj, J. O. Richardson, F. Paesani, *Nat. Chem.* **11**, 367 (2019).

[9] P. F. Bernath, *Spectra of Atoms and Molecules (Second Edition)* (Oxford University Press, New York, 2005).

[10] S. Mukamel, *Principles of Nonlinear Optical Spectroscopy* (Oxford University Press, 1999).

[11] E. B. Wilson, J. C. Decius, P. C. Cross, *Molecular Vibrations: The Theory of Infrared and Raman Vibrational Spectra* (Dover Publications, Mineola, NY, USA, 1980).

[12] S. Guo, M. A. Watson, W. Hu, Q. Sun, G. K.-L. Chan, *J. Chem. Theory Comput.* **12**, 1583 (2016).

[13] J. Vázquez, J. F. Stanton, *Mol. Phys.* **105**, 101 (2007).

[14] E. L. Sibert, D. P. Tabor, N. M. Kidwell, J. C. Dean, T. S. Zwier, *J. Phys. Chem. A* **118**, 11272 (2014).

[15] A. B. McCoy, T. L. Guasco, C. M. Leavitt, S. G. Olesen, M. A. Johnson, *Phys. Chem. Chem. Phys.* **14**, 7205 (2012).

[16] L. B. Harding, Y. Georgievskii, S. J. Klippenstein, *J. Phys. Chem. A* **121**, 4334 (2017).

[17] G.-L. Hou, *et al.*, *J. Phys. Chem. Lett.* **4**, 779 (2013).

[18] V. Barone, M. Biczysko, C. Puzzarini, *Acc. Chem. Res.* **48**, 1413 (2015).

[19] B. A. McGuire, *et al.*, *Science* **359**, 202 (2018).

[20] S. Ospelkaus, *et al.*, *Phys. Rev. Lett.* **104**, 030402 (2010).

[21] R. F. Ribeiro, L. A. Martinez-Martinez, M. Du, J. Campos-Gonzalez-Angulo, J. Yuen-Zhou, *Chem. Sci.* **9**, 6325 (2018).

[22] V. Kapil, E. Engel, M. Rossi, M. Ceriotti, *J. Chem. Theory Comput.* **15**, 5845 (2019).

[23] A. J. Leggett, *Quantum Liquids: Bose Condensation and Cooper Pairing in Condensed-Matter Systems* (Oxford University Press, 2006), first edn.

[24] J. Huh, G. G. Guerreschi, B. Peropadre, J. R. Mcclean, A. Aspuru-Guzik, *Nat. Photonics* **9**, 615 (2015).

[25] C. Sparrow, *et al.*, *Nature* **557**, 660 (2018).

[26] S. Joshi, A. Shukla, H. Katiyar, A. Hazra, T. S. Mahesh, *Phys. Rev. A* **90**, 022303 (2014).

[27] A. Teplukhin, B. K. Kendrick, D. Babikov, *J. Chem. Theory Comput.* **15**, 4555 (2019).

[28] R. J. MacDonell, *et al.*, *arXiv* (2020). arXiv:2012.01852.

[29] N. P. D. Sawaya, J. Huh, *J. Phys. Chem. Lett.* **10**, 3586 (2019).

[30] P. J. Ollitrault, A. Baiardi, M. Reiher, I. Tavernelli, *Chem. Sci.* **11**, 6842 (2020).

[31] L. Veis, J. Višňák, H. Nishizawa, H. Nakai, J. Pittner, *Int. J. Quantum Chem.* **116**, 1328 (2016).

[32] A. Macridin, P. Spentzouris, J. Amundson, R. Harnik, *Phys. Rev. Lett.* **121**, 110504 (2018).

[33] A. B. Magann, M. D. Grace, H. A. Rabitz, M. Sarovar, *arXiv* (2020). arXiv:2002.12497.

[34] P. J. Ollitrault, G. Mazzola, I. Tavernelli, *arXiv* (2020). arXiv:2006.09405.

[35] T. Kosugi, Y.-i. Matsushita, *Phys. Rev. Research* **2**, 033043 (2020).

[36] X. Cai, W.-H. Fang, H. Fan, Z. Li, *arXiv* (2020). arXiv:2001.03406.

[37] R. Somma, G. Ortiz, E. Knill, J. Gubernatis, *arXiv* (2003). arXiv:quant-ph/0304063.

[38] N. P. D. Sawaya, *et al.*, *npj Quantum Inf.* **6**, 49 (2020).

[39] N. P. D. Sawaya, G. G. Guerreschi, A. Holmes, *2020 IEEE International Conference on Quantum Computing and Engineering (QCE)* (IEEE, 2020).

[40] J. R. McClean, J. Romero, R. Babbush, A. Aspuru-Guzik, *New J. Phys.* **18**, 023023 (2016).

[41] T.-C. Yen, R. A. Lang, A. F. Izmaylov, *The J. Chem. Phys.* **151**, 164111 (2019).

[42] J. M. Bowman, T. Carrington, H.-D. Meyer, *Mol. Phys.* **106**, 2145 (2008).

[43] J. C. Light, Z. Bačić, *J. Chem. Phys.* **87**, 4008 (1987).

[44] E. L. Sibert, *J. Chem. Phys.* **88**, 4378 (1988).

[45] X.-G. Wang, T. Carrington, *J. Chem. Phys.* **129**, 234102 (2008).

[46] A. van der Avoird, D. J. Nesbitt, *J. Chem. Phys.* **134**, 044314 (2011).

[47] Z. Lin, A. B. McCoy, *J. Phys. Chem. A* **119**, 12109 (2015).

[48] G. Simons, R. G. Parr, J. M. Finlan, *J. Chem. Phys.* **59**, 3229 (1973).

[49] J. Zúñiga, J. A. G. Picón, A. Bastida, A. Requena, *J. Chem. Phys.* **122**, 224319 (2005).

[50] I. W. Bulik, M. J. Frisch, P. H. Vaccaro, *J. Chem. Phys.* **147**, 044110 (2017).

[51] D. Poulin , P. Wocjan, *Phys. Rev. Lett.* **103**, 220502 (2009).

[52] A. Riera, C. Gogolin, J. Eisert, *Phys. Rev. Lett.* **108**, 080402 (2012).

[53] M. Motta, *et al.*, *Nat. Phys.* **16**, 205 (2019).

[54] A. N. Chowdhury, G. H. Low, N. Wiebe, *arXiv* (2020). arXiv:2002.00055.

[55] Y. Wang, G. Li, X. Wang, *arXiv* (2020). arXiv:2005.08797.

[56] O. Higgott, D. Wang, S. Brierley, *Quantum* **3**, 156 (2019).

[57] T. Jones, S. Endo, S. McArdle, X. Yuan, S. C. Benjamin, *Phys. Rev. A* **99**, 062304 (2019).

[58] L.-W. Wang, A. Zunger, *J. Chem. Phys.* **100**, 2394 (1994).

[59] P. J. Ollitrault, *et al.*, *arXiv* (2019). arXiv:1910.12890.

[60] V. Havlíček, *et al.*, *Nature* **567**, 209 (2019).

[61] H. Buhrman, R. Cleve, J. Watrous, R. de Wolf, *Phys. Rev. Lett.* **87**, 167902 (2001).

[62] J. C. Garcia-Escartin, P. Chamorro-Posada, *Phys. Rev. A* **87**, 052330 (2013).

[63] K. Mitarai, K. Fujii, *Phys. Rev. Research* **1**, 013006 (2019).

[64] Y. Ibe, *et al.*, *arXiv* (2020). arXiv:2002.11724.

[65] M. A. Nielsen, I. L. Chuang, *Quantum Computation and Quantum Information: 10th Anniversary Edition* (Cambridge University Press, New York, NY, USA, 2011), 10th edn.

[66] N. P. D. Sawaya, M. Smelyanskiy, J. R. McClean, A. Aspuru-Guzik, *J. Chem. Theory Comput.* **12**, 3097 (2016).

[67] J. Romero, *et al.*, *Quantum Sci. Technol.* **4**, 014008 (2018).

[68] S. Endo, S. C. Benjamin, Y. Li, *Phys. Rev. X* **8**, 031027 (2018).

[69] J. R. McClean, Z. Jiang, N. C. Rubin, R. Babbush, H. Neven, *Nat. Commun.* **11**, 636 (2020).

[70] K. Sharma, S. Khatri, M. Cerezo, P. J. Coles, *New J. Phys.* **22**, 043006 (2020).

[71] J. R. McClean, M. E. Kimchi-Schwartz, J. Carter, W. A. de Jong, *Phys. Rev. A* **95**, 042308 (2017).

[72] R. Santagati, *et al.*, *Sci. Adv.* **4**, eaap9646 (2018).

[73] D. Wecker, *et al.*, *Phys. Rev. A* **92**, 062318 (2015).

[74] A. Roggero, J. Carlson, *Phys. Rev. C* **100**, 034610 (2019).

[75] L. K. Grover, *Proceedings of the twenty-eighth annual ACM symposium on Theory of computing - STOC 96* (ACM Press, 1996).

[76] L. K. Grover, *Phys. Rev. Lett.* **80**, 4329 (1998).

[77] A. M. Childs, D. Maslov, Y. Nam, N. J. Ross, Y. Su, *Proc. Natl. Acad. Sci.* **115**, 9456 (2018).

[78] R. C. Fortenberry, X. Huang, A. Yachmenev, W. Thiel, T. J. Lee, *Chem. Phys. Lett.* **574**, 1 (2013).

[79] E. L. Sibert, *J. Chem. Phys.* **150**, 090901 (2019).

[80] R. Babbush, *et al.*, *Phys. Rev. X* **8**, 011044 (2018).

[81] R. Babbush, *et al.*, *Phys. Rev. X* **8**, 041015 (2018).

[82] D. W. Berry, C. Gidney, M. Motta, J. R. McClean, R. Babbush, *Quantum* **3**, 208 (2019).

[83] V. von Burg, *et al.*, *arXiv* (2020). arXiv:2007.14460.

[84] P. Jordan, E. Wigner, *Z. Angew. Phys.* **47**, 631 (1928).

[85] S. B. Bravyi, A. Y. Kitaev, *Ann. Phys.* **298**, 210 (2002).

[86] D. W. Berry, A. M. Childs, R. Kothari, *2015 IEEE 56th Annual Symposium on Foundations of Computer Science* (2015), pp. 792–809.

[87] D. W. Berry, A. M. Childs, R. Cleve, R. Kothari, R. D. Somma, *Phys. Rev. Lett.* **114**, 090502 (2015).

[88] G. H. Low, I. L. Chuang, *Phys. Rev. Lett.* **118**, 010501 (2017).

[89] A. M. Childs, Y. Su, M. C. Tran, N. Wiebe, S. Zhu, *arXiv* (2019). arXiv:1912.08854.

[90] J. F. Gonthier, *et al.*, *arXiv* (2020). arXiv:2012.04001.

[91] M. Reiher, N. Wiebe, K. M. Svore, D. Wecker, M. Troyer, *Proc. Natl. Acad. Sci.* **114**, 7555 (2017).

[92] Z. Li, J. Li, N. S. Dattani, C. J. Umrigar, G. K.-L. Chan, *arXiv* (2018). arXiv:1809.10307.

[93] V. E. Elfving, *et al.*, *arXiv* (2020). arXiv:2009.12472.

[94] J. P. Heindel, K. M. Herman, E. Aprà, S. S. Xantheas, *The J. Phys. Chem. Lett.* **12**, 7574 (2021).

[95] L. Gyevi-Nagy, M. Kállay, P. R. Nagy, *J. Chem. Theory Comput.* **16**, 366 (2019).

[96] J. R. McClean, *et al.*, *Quantum Sci. Technol.* **5**, 034014 (2020).

[97] P. Virtanen, *et al.*, *Nat. Methods* **17**, 261 (2020).

[98] S. McArdle, *et al.*, *npj Quantum Inf.* **5**, 75 (2019).

[99] K.-S. Lee, U. R. Fischer, *Int. J. Mod. Phys. B* **28**, 1550021 (2014).

[100] M. P. Woods, M. Cramer, M. B. Plenio, *Phys. Rev. Lett.* **115**, 130401 (2015).

[101] T. Helgaker, P. Jorgensen, J. Olsen, *Molecular Electronic-Structure Theory* (Wiley, 2013).

[102] R. M. Parrish, *et al.*, *J. Chem. Theory Comput.* **13**, 3185 (2017).

[103] V. Kapil, E. Engel, M. Rossi, M. Ceriotti, *J. Chem. Theory Comput.* **15**, 5845 (2019).

[104] S. Sharma, T. Yanai, G. H. Booth, C. J. Umrigar, G. K.-L. Chan, *The J. Chem. Phys.* **140**, 104112 (2014).

[105] W. J. Huggins, *et al.*, *arXiv* (2019). arXiv:1907.13117.

[106] C. J. Cramer, *Essentials of Computational Chemistry: Theories and Models* (Wiley, 2004), first edn.

[107] D. A. Matthews, *et al.*, *J. Chem. Phys.* **152**, 214108 (2020).

[108] A. Barbe, C. Secroun, P. Jouve, *J. Mol. Spectrosc.* **49**, 171 (1974).

[109] S. M. Adler-Golden, S. R. Langhoff, C. W. Bauschlicher, G. D. Carney, *J. Chem. Phys.* **83**, 255 (1985).

Appendix A: Vibrational operators and mappings to qubits

Both the Hamiltonian and $\mu^{(\alpha)}$ must be mapped to a set of qubits. The operator for a single d-level particle (included a truncated bosonic mode) may be expressed as

$$A = \sum_{l,l'=0}^{d-1} c_{l,l'} |l'\rangle\langle l|. \tag{A1}$$

In order to use a qubit-based quantum computer, each level must first be mapped to a bit representation, before the operator is mapped to a sum of products of Pauli matrices. For example, a 4-level particle with an operator $B = |2\rangle\langle 3| + |3\rangle\langle 2|$ would map to

$$|2\rangle\langle 3| + |3\rangle\langle 2| \xrightarrow{\text{Std. Binary}} |10\rangle\langle 11| + |11\rangle\langle 10|$$

$$= |1\rangle\langle 1| \otimes |0\rangle\langle 1| + |1\rangle\langle 1| \otimes |1\rangle\langle 0| \tag{A2}$$

$$= \frac{1}{2}\left(\hat{X}_0 - \hat{Z}_1\hat{X}_0\right)$$

where the least significant bit (qubit) is labelled 0. In the last step, the following identities are used: $|0\rangle\langle 1| = \frac{1}{2}(\hat{X} + i\hat{Y})$; $|1\rangle\langle 0| = \frac{1}{2}(\hat{X} - i\hat{Y})$; $|0\rangle\langle 0| = \frac{1}{2}(I + \hat{Z})$; and $|1\rangle\langle 1| = \frac{1}{2}(I - \hat{Z})$.

In the case of vibrational (bosonic) degrees of freedom, one would truncate at a level of d that preserves the accuracy one requires [99, 100]. We use the Gray code for the numerics presented in this work; for a more thorough study of the choice and tradeoffs for different mappings, see reference [38].

Appendix B: Counting for fermionic operators

Here we summarize how the Pauli string counts were determined for molecular Hamiltonians. The electronic structure Hamiltonian takes the form

$$H_{ES} = \sum_{p\sigma q\tau} h_{p\sigma,q\tau} a_{p\sigma}^\dagger a_{q\tau} + \sum_{pqrs\sigma\tau\mu\nu} h_{p\sigma,r\mu,s\nu,q\tau} a_{p\sigma}^\dagger a_{r\mu}^\dagger a_{s\nu} a_{q\tau} \tag{B1}$$

where Latin letters label spatial orbitals and Greek letters label the spin.

We assume that a real (as opposed to complex) basis is used. Fermionic commutation rules and spin orthogonality lead to the following symmetries [101]. First,

$$h_{PQRS} = h_{RSPQ} \tag{B2}$$

and

$$h_{PQRS} = h_{QPRS} = h_{PQSR} = h_{QPSR}, \tag{B3}$$

which leads to an eight-fold symmetry. Including orthogonality of spin degrees of freedom leads to

$$h_{p\sigma,q\tau,r\mu,s\nu} = h_{pqrs}\delta_{\sigma\tau}\delta_{\mu\nu}. \tag{B4}$$

Finally, the following terms vanish:

$$\{a_i^\dagger a_i^\dagger a_j a_j, a_j^\dagger a_j^\dagger a_i a_i\} \to 0, \tag{B5}$$

$$a_i^\dagger a_i^\dagger a_i a_i \to 0, \tag{B6}$$

$$a_i^\dagger a_i^\dagger a_j a_k \to 0. \tag{B7}$$

For each category of fermionic Hamiltonian term, we now consider the number of Pauli strings resulting from the Jordan-Wigner mapping, though the Pauli string count (but not the locality) is the same for the Bravyi-Kitaev mapping. The Jordan-Wigner encoding maps fermionic degrees of freedom to qubits such that fermionic commutation relations are retained. The mapping is defined as

$$a_p^\dagger \mapsto \left(\prod_{m<p} Z_m\right) \sigma_p^+$$
$$a_p^\dagger \mapsto \left(\prod_{m<p} Z_m\right) \sigma_p^- \tag{B8}$$

where $\sigma^\pm \equiv (X \mp iY)/2$.

In our counting procedure, we avoid double-counting Pauli terms. For instance, terms like Z_i appear in both one- and two-electron operators, but they are counted only once.

The one-electron terms lead to

$$a_i^\dagger a_i \to Z + I = \frac{1}{2}(I - Z_i) \tag{B9}$$

and

$$a_i^\dagger a_j + a_j^\dagger a_i \to \frac{1}{2}(X_i Z^{\otimes j-i-1} X_j + Y_i Z^{\otimes j-i-1} Y_j). \tag{B10}$$

Non-vanishing two-orbital two-electron terms lead to

$$a_i^\dagger a_j^\dagger a_j a_i + a_j^\dagger a_i^\dagger a_i a_j \rightarrow \{I, Z_i, Z_j, Z_i Z_j\} \tag{B11}$$

Based on the above symmetries, non-vanishing three-orbital terms lead to

$$\{a_i^\dagger a_j^\dagger a_k a_i, \cdots\}_{(4)} \cup \{a_i^\dagger a_j^\dagger a_i a_k, \cdots\}_{(4)} \rightarrow 4 \text{ Pauli strings}$$

$$\text{Example: } \{a_0^\dagger a_1^\dagger a_2 a_0, \cdots\}_{(4)} \cup \{a_0^\dagger a_1^\dagger a_0 a_2, \cdots\}_{(4)} \tag{B12}$$

$$\rightarrow \{Z_0 X_2 X_3, Z_0 Y_2 Y_3, X_2 X_3, Y_2 Y_3\}$$

where each set of four operators leads to the same set of Pauli strings. Subscripts denote the number of Pauli strings in the bracketed set.

Finally, consider four-orbital terms with 8-fold symmetry. One such set of terms leads to four Pauli strings:

$$\{a_i^\dagger a_k^\dagger a_l a_j, \cdots\}_{(4)} \rightarrow 4 \text{ Pauli strings}$$

$$\text{Example: } \{a_1^\dagger a_3^\dagger a_5 a_7, ...\}_{(4)} \rightarrow \{X_1 Z_2 X_3 Y_5 Z_6 Y_7,$$

$$X_1 Z_2 Y_3 Y_5 Z_6 X_7, \tag{B13}$$

$$Y_1 Z_2 X_3 X_5 Z_6 Y_7,$$

$$Y_1 Z_2 Y_3 X_5 Z_6 X_7\})$$

The above formulas were used to write a simple function that "manually" counts the upper bound to the number of Pauli terms in electronic structure problems for a given number of orbitals. Next, to numerically validate our manual counting procedure, we used OpenFermion [96] and Psi4 [102] to calculate the number of Pauli strings required for the electronic structure problem of a collection of hydrogen atoms. Hydrogen atoms were placed on a cubic lattice with spacing 0.6 Å, with a random perturbation in each direction drawn from a Gaussian of standard deviation 0.05 Å. We used the minimal STO-3G basis, resulting in a number of qubits equal to 4 times the number of hydrogen atoms. The canonical orbitals used were determined from the Hartree-Fock calculation of Psi4. All Pauli string counts were within 10% to 30% of our manual analytical counts, a difference that we attribute primarily to the software truncating terms smaller than 10^{-6}.

26

Appendix C: Counting for bosonic operators

All of our mappings use the Gray code [38]. Here we provide the Pauli mappings or Pauli counts for the different types of many-body terms, for both $d=4$ and 8. These are used for counting the number of terms in each type of Hamiltonian.

Harmonic:

$$\begin{aligned}
p_0^2 + q_0^2 &\xrightarrow{d=4} 4I - 1Z_0Z_1 - 2Z_1 \\
&\xrightarrow{d=8} 8I - 1Z_0Z_1Z_2
\end{aligned} \tag{C1}$$

3rd-order:

$$\begin{aligned}
q_i^3 &\xrightarrow{d=4} \{X_0, X_0Z_1, Z_0X_1, X_1\} \\
&\xrightarrow{d=8} (16 \text{ Pauli strings})
\end{aligned} \tag{C2}$$

$$\begin{aligned}
q_i^2 q_j &\xrightarrow{d=4} (20 \text{ Pauli strings}) \\
&\xrightarrow{d=8} (144 \text{ Pauli strings})
\end{aligned} \tag{C3}$$

4th-order:

$$\begin{aligned}
q_i^4 &\xrightarrow{d=4} (I \ \& \ 5 \text{ Pauli strings}) \\
&\xrightarrow{d=8} (I \ \& \ 18 \text{ Pauli strings})
\end{aligned} \tag{C4}$$

$$\begin{aligned}
q_i^3 q_j &\xrightarrow{d=4} (16 \text{ Pauli strings}) \\
&\xrightarrow{d=8} (192 \text{ Pauli strings})
\end{aligned} \tag{C5}$$

$$\begin{aligned}
q_i^2 q_j^2 &\xrightarrow{d=4} (I \ \& \ 24 \text{ Pauli strings}) \\
&\xrightarrow{d=8} (144 \text{ Pauli strings})
\end{aligned} \tag{C6}$$

$$\begin{aligned}
q_i^2 q_j q_k &\xrightarrow{d=4} (80 \text{ Pauli strings}) \\
&\xrightarrow{d=8} (1728 \text{ Pauli strings})
\end{aligned} \tag{C7}$$

The above formulas were used to write a function that manually counts the number of Pauli strings, for a given truncation d and number of modes. In order to numerically
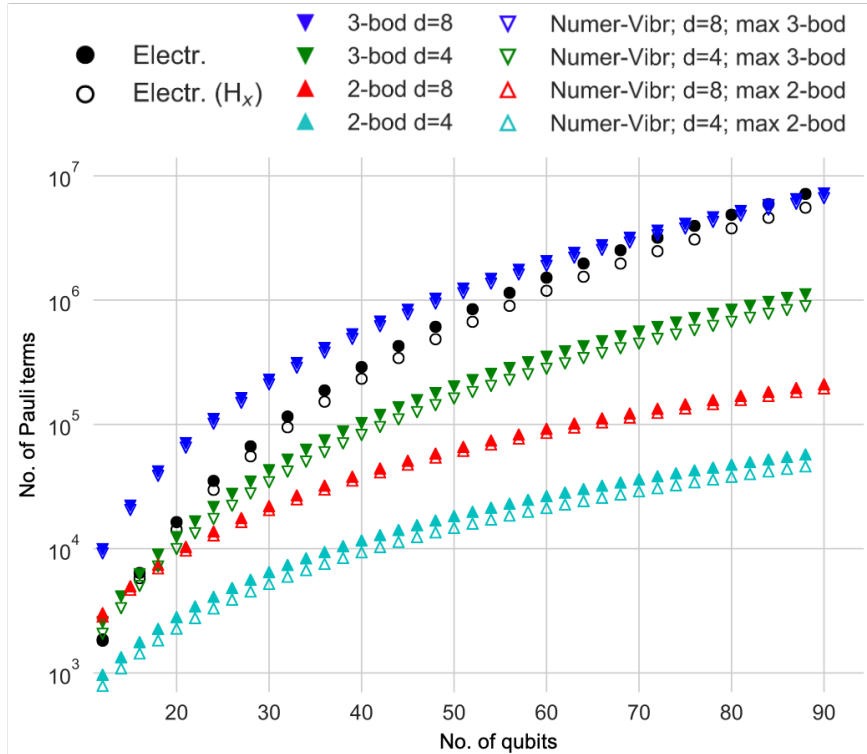
27

FIG. 4. Pauli string counts, including both analytical ("manual") and numerical (random vibrational Hamiltonian) results.

validate our counting procedure, we prepared model vibrational Hamiltonians with randomized non-zero couplings for all possible second-, third-, and fourth-order terms. These model Hamiltonians represent the *worst* possible case, are used only for counting terms, and do not correspond to real molecules; real-world Hamiltonians are used only for the four problems solved later in the paper. After creating the model Hamiltonians, we used the automated procedure described in Section A and previous work [38]. As in the case of the electronic results, we attribute discrepancies with our analytic results to the software's truncation of intermediate terms smaller than 10^{-6}. We omitted these "numerical" vibrational results from the main text in order to avoid over-crowding the figure. The analytical and numerical results for all Hamiltonians are shown in Figure 4.

Appendix D: Coefficients and precision

As discussed in the main text, for both near- and long-term Hamiltonian simulation the required computational resources depend partly on the desired precision and some measure

of the Hamiltonian's magnitude (such as a matrix norm). For instance, as Gonthier et al. recently pointed out [90], it is not just the Pauli counts and lengths but also the coefficients of each term that are relevant to determining computational resource estimates. Their work mentioned this in the context of the measurements required for VQE, though it is true for most other Hamiltonian simulation techniques as well.

For a set of electronic and vibrational Hamiltonians described below, we calculate the following quantity (reproduced from the main text) as a way to compare matrix magnitudes:

$$W = \sqrt{\sum_{k \neq k_I} a_k^2}, \tag{D1}$$

where $k \neq k_I$ signifies that the coefficient in front of the identity operator is excluded. $W 2^{N_q/2}$ is an upper bound to the Frobenius norm, defined as $|H|_F = \sqrt{\sum b_{ij}^2}$, where b_{ij} is element of the ith row and jth column of the Hamiltonian. We choose this metric because it is trivial to calculate and because it directly relates to resource estimates, such as the number of measurements required in VQE [90].

It is beyond the scope of this work to provide actual resource estimates, as extensive calculations and the choice of specific molecules would be needed (indeed, entire studies have been dedicated estimating resources for a few molecules or a single molecule [91–93]). Instead, we have considered three metrics that are rough proxies for computational complexity: term counts, Pauli length, and W. Support for our postulate of vibrational quantum advantage comes from the fact that these approximations (which are pessimistic for the vibrational case) show approximately an order of magnitude smaller values (in term counts and in W), for problems larger than 40 qubits.

As stated, we used pessimistic assumptions to construct vibrational Hamiltonians, partly in order to mitigate the fact the electronic structure calculations are approximate models. As before, we include up to either 2- or 3-body mode coupling terms and $d = \{4, 8\}$. Harmonic modes were set to evenly spaced values from 1000 to 4000 cm^{-1}. Every possible third-order term was given a coefficient of 400 cm^{-1} and every possible fourth-order term given 40 cm^{-1}. It is unlikely that a molecule would include such dense mode coupling, and the first vibrational problem to exhibit quantum advantage will by definition be a problem with lower coupling density.

For electronic structure, our goal was to obtain order-of-magnitude estimates for some chemical elements that might be the first to see quantum advantage. It is reasonable to

speculate [91, 93] that the first electronic structure simulation to show quantum advantage will be for a molecule containing transition metal elements, because the classical coupled cluster algorithm class, *e.g.* CCSD(T), accurately treats many main group molecules (*e.g.* hydrocarbons and water clusters) up to more than a thousand orbitals [93–95]. CCSD(T) and other state-of-the-art methods often cannot accurately treat molecules with transition metal elements, which is part of the reason that quantum computational resource estimates to date have focused on such compounds [91–93]. Notably, the toy H_x (hydrogen box) model we used to calculate term counts in fact showed much *greater* values of W than those of the transition elements, though H_x is not a particularly useful chemical system and may not require a quantum computer to begin with.

We created simple electronic structure models of twelve transition metal molecules: V_x, Cr_x, Mn_x, Fe_x, where $x \in \{2, 3, 4\}$ and closed-shell anions were used for V_3^- and Mn_3^-. All molecules were constrained to have singlet multiplicity. Using a minimal STO-3G basis, we ran OpenFermion [96] and Psi4 [102] to determine the canonical orbitals. We then froze the canonical orbitals corresponding to atomic orbitals $1s^2\ 2s^2\ 2p^6\ 3s^2\ 3p^6$. We chose an active space of 6 orbitals (12 spin-orbitals) per atom, the lowest-energy orbitals excluding the frozen core.

As is well known to chemists but perhaps less well-known in the physics community, different chemistry applications require dramatically different precisions. A qualitative understanding of some electronic structure problems may require a low accuracy of just 10 milliHartrees (mHa), thermodynamics observables (for both electronic and vibrational calculations) often require an accuracy of 1 mHa, and interpreting transition lines in a vibrational spectrum may require precisions as low as 5 μHa.

Table I shows matrix magnitudes W and the maximum non-identity Pauli coefficient for each Hamiltonian. W ought to be compared only between Hamiltonians of the same qubit count. The far right columns in table I give the quotient W/ϵ for three different values of ϵ. As different applications require different levels of precision, this quotient is useful because it provides a comparison between matrix magnitude and ϵ. Time complexity for different Hamiltonian simulation algorithms are dependent on both ϵ and matrix magnitude [77, 86–89], though the relationship is non-trivial and normally uses a more standard metric of matrix magnitude such as the spectral norm.

As a sanity check we show the maximum Pauli coefficient of a published fermionic Hamil-

tonian for the FeMoco cofactor (Li *et al.* [92]), a widely studied biological molecule containing several transition metal elements. We include this value because their careful procedure for choosing the orbitals and active space is nearer to what one would do for a real quantum calculation. We are cautious not to make direct comparisons, due to the higher qubit counts (154 qubits) and presence of the fifth-row element molybdenum.

The first ϵ of 100 cm^{-1} $\approx$ 0.455 mHa is just below "chemical accuracy" of 1.6 mHa, an energy precision that is acceptable for many applications. The stated goal of many electronic structure calculations, including above-mentioned work in quantum computational resource estimates, is to achieve sub-chemical accuracy. This is a reasonable goal for electronic structure calculations containing transition metals. Notably, $k_B T$ is $\sim$0.6 kcal/mol or $\sim$209 cm^{-1}at room temperature, implying that thermal fluctuations in a typical laboratory are on the same order as this common standard for computational accuracy.

There will be molecules and complexes for which a highly accurate PES may be achieved using CCSD(T) or other methods, but for which the vibrational zero-point energy (ZPE) is classically intractable [16, 103]. Calculating this ground-state energy (*i.e.* ZPE) is a good first place to look for quantum advantage, because it might require no better than chemical accuracy (discussed below) for some applications. However, if a quantum device is capable of solving ZPE, the device is not far from being able to calculate low-lying transitions. Only a doubling of depth (or alternatively a doubling of qubits) would be required in order to use the variational quantum deflation method to obtain low-lying excited states and transitions [56].

Notably, "chemical accuracy" of 1.6 mHa is not sufficient for some applications. For instance, because of the exponential behavior of the Arrhenius equation, rate constants may be incorrect by about an order of magnitude. Another example for which chemical accuracy is insufficient is vibrational eigenstates, between which the spacing is often much smaller than 100 cm^{-1}.

The higher accuracy of 1 cm^{-1} $\approx$ 4.55 μHa is sometimes referred to as spectroscopic accuracy, though the term does not have a universally accepted definition [5, 78, 104]. The important point is that the interpretation of vibrational spectra often requires a high accuracy of between 1 cm^{-1} and 10 cm^{-1}. Notably, when a PES is being calculated using electronic structure, the accuracy of the PES cannot be worse than the accuracy required for the spectroscopic problem.

It is not just the precision and the norm or magnitude of the Hamiltonian, but also its locality that determines the required resources. Complexity theoretic results have shown that a more local Hamiltonian will require fewer resources [77, 86–89]. Hence the advantage from the lower magnitude of the vibrational Hamiltonians will be improved even further relative to electronic Hamiltonians due to the lower locality, suggesting that focusing only on W is again pessimistic against the vibrational case.

A comment on the number of measurements required in VQE is merited as well. Gonthier *et al.* recently studied the number of measurements required for estimating the electronic energy of a set of organic molecules [90]. The quantity W is closely related to the factor that Gonthier *et al.* calculate to determine measurement counts. If one were to take the naive route of measuring only one Pauli term expectation value per circuit run, then $(W/\epsilon)^2$ would be proportional to the number of measurements. (As a side note, we do not necessarily consider the number of measurements to be the limiting factor for VQE. We would argue that the primary concern for near-term hardware should be circuit depth, which would also be dependent on desired accuracy. Measurements in principle can be parallelized across devices; on the other hand, if the required circuit depth is too great for the hardware, there is little one can do.)

In practice, for the near-term VQE algorithm one desires as few circuit runs as possible. Gonthier *et al.* report numerical results fitted to a simple power law, showing for a set of organic molecules that the number of required measurements growing as $\mathcal{O}(N_q^{5.1})$ to $\mathcal{O}(N_q^{5.8})$ when Pauli terms are grouped together, and growing as $\mathcal{O}(N_q^{2.3})$ to $\mathcal{O}(N_q^{3.6})$ when using the so-called basis rotation grouping [90, 105]. (The latter method requires additional circuit depth that grows with the number of qubits, appended to the end of the state preparation ansatz.)

For vibrational Hamiltonians, on the other hand, the number of VQE circuit repetitions for two-body vibrational Hamiltonians is upper bounded by $\mathcal{O}(N_q^1)$. This is because two-body terms can be measured simultaneously; one may measure terms on modes $((0,1),(2,3),\cdots)$ followed by $((0,2),(1,3),\cdots)$ and so on, where integer pairs correspond to mode pairs. Analogously, the number of circuit repetitions for three-body vibrational Hamiltonians scale at worst as $\mathcal{O}(N_q^2)$. Hence both the lower values of W and the apparently lower measurement scaling suggest that fewer measurements will be required for the vibrational case, for a given precision.

In summary, the three quantities of term count, locality, and W suggest that vibrational problems will require fewer quantum resources for a given precision. As chemical accuracy (order of ~ 1 mHa) is required for order-of-magnitude accuracy in rate constants (due to the Arrhenius equation [106]) regardless of which which type of degree of freedom is being simulated, we suggest that vibrational zero-point energy calculations and/or low-lying vibrational transitions are a reasonable place to look for early quantum advantage.

Appendix E: Comparing Hamiltonians

We use this section to elaborate on some points made in the main text, regarding comparisons between vibrational and electronic problems.

Note that the 3rd- and 4th-order vibrational Taylor terms in H_{anharm} (defined in the main text) in fact yield at most 2- and 3-body interactions, respectively, as every higher-order term necessarily includes q_i^2 in the product if one is using normal modes. This leads to either a $\mathcal{O}(M^2)$ or $\mathcal{O}(M^3)$ scaling in the number of terms for this subset of molecules, compared to $\mathcal{O}(N^4)$ for electronic structure of an arbitrary molecule, where N is the number of spin-orbitals. Though we discuss high-lying excited states in our work, note that for this consideration of quantum advantage we are assuming that only low-lying vibrational states are being calculated. Very high-lying vibrational states may require larger numbers of vibrational levels or the use of more costly methods such as folded Hamiltonians.

It is important to point out that one should assume that state-of-the-art methods will be used to reduce the number of qubits required to simulate *whichever* problem is considered, leading to substantial reductions in the number of effective vibrational modes or electronic orbitals. In vibrational problems, one may choose a coordinate system that is efficient in terms of having low truncation requirements and fewer appreciable coupling terms [11, 79]. For electronic structure, one carefully chooses the active space of orbitals [83, 91, 92]. The point is, the use of "qubit reduction" methods does not change the overall argument unless the modified problem changes one of the stated criteria, *e.g.* if the problem is no longer well-described by a fourth-order Hamiltonian, in which case we exclude such a problem from the discussion anyway. Methods for reducing qubit count in electronic structure should intuitively still produce a Hamiltonian with a similar number of terms and with similar magnitude. The appropriate comparison to make is still between two Hamiltonians of similar

qubit counts. Further, it may be the case that some qubit reduction techniques would work equally well for bosonic and fermionic problems.

Note that several encoding choices are possible. Instead of using the Gray code, one may choose to use the unary encoding (also called direct mapping or one-hot encoding) with vibrational degrees of freedom, which would tend to reduce circuit depth at the expense of increasing the number of qubits [3, 38]. We note that if we had used the unary encoding, the Hamiltonians would have been even simpler (fewer terms and shorter Pauli lengths, and similar matrix magnitude W). In principle this simpler Hamiltonian would either strengthen our conclusion (because the Hamiltonian can be simulated in shorter depth) or be a moot case (if the unary mapping requires too many qubits for whatever device characteristics you happen to be assuming).

Finally, we stress again that our argument holds for only some subset of vibrational problems; some vibrational problems would require inclusion of *e.g.* four- or five-body terms for accurate simulation, and some vibrational problems require more coupling terms than others.

Appendix F: Potential energy surfaces and dipole surfaces

The potential energy surface and dipole derivatives for CO and COH were calculated at the CCSD(T)/ANO1 level with the CFOUR package, version 2.1 [107]. We used the package's documented scripts for calculating anharmonic frequencies by finite difference. Energies were calculated in parallel to obtain the quadratic, cubic, and quartic (including three-body) force constants, all automatically produced by CFOUR during the anharmonic frequency calculations.

All energy units below are in cm^{-1}. The resulting fourth-order Hamiltonian for carbon monoxide is

$$H_{CO} = 2157.96\frac{q^2 + p^2}{2} - 736.66\ q^3 + 210.97\ q^4. \tag{F1}$$

The fourth-order Hamiltonian for the isoformyl radical is

$$H_{COH} = 1143.24 \frac{q_1^2 + p_1^2}{2} + 1393.46 \frac{q_2^2 + p_2^2}{2} + 3530.65 \frac{q_3^2 + p_3^2}{2}$$

$$+ -16.83 \; q_1q_1q_1 + 51.76 \; q_1q_1q_2 + 40.02 \; q_1q_2q_2 + 87.05 \; q_2q_2q_2$$

$$+ 413.74 \; q_1q_1q_3 - 116.13 \; q_1q_2q_3 - 35.26 \; q_2q_2q_3 - 92.65 \; q_1q_3q_3$$

$$- 119.29 \; q_2q_3q_3 - 489.34 \; q_3q_3q_3 + 22.83 \; q_1q_1q_1q_1 - 10.84 \; q_1q_1q_1q_2$$

$$- 10.48 \; q_1q_1q_1q_3 - 0.49 \; q_1q_1q_2q_2 - 40.20 \; q_1q_1q_2q_3 - 252.07 \; q_1q_1q_3q_3 \qquad \text{(F2)}$$

$$+ 7.00 \; q_1q_2q_2q_2 - 3.37 \; q_1q_2q_2q_3 + 6.96 \; q_2q_2q_2q_2 - 6.15 \; q_2q_2q_2q_3$$

$$- 17.44 \; q_2q_2q_3q_3 + 26.32 \; q_1q_2q_3q_3 - 3.13 \; q_1q_3q_3q_3 - 4.33 \; q_2q_3q_3q_3$$

$$+ 66.64 \; q_3q_3q_3q_3,$$

where q_1 is the bending mode, q_2 is the CO stretch, and q_3 is the OH stretch.

The first-order transition dipoles were found to be

$$\mu^{(x)} \sim -0.33854 \; q_1 - 0.268687 \; q_2 - 0.011334 \; q_3$$

$$\mu^{(y)} \sim -0.057874 \; q_1 - 0.023912 \; q_2 + 0.175823 \; q_3 \qquad \text{(F3)}$$

where the equilibrium dipole is irrelevant because it cancels out due to orthogonality. Units are in Debye, though we considered only relative intensities in our calculations.

For ozone (isotope $^{16}O_3$) we used previously published PES [108] and DMSs [109].

Our model Hamiltonian for Fermi resonances has two vibrational modes, taking the form

$$\hat{H}_{FR} = \omega_0 \left(a_0^\dagger a_0 + \frac{1}{2} \right) + \omega_1 \left(a_1^\dagger a_1 + \frac{1}{2} \right) + h_{001} q_0^2 q_1 \qquad \text{(F4)}$$

We choose frequencies and couplings that are typical for the bending and stretching modes of two CH stretches within a methyl (CH_3) functional group, a well-known example of Fermi resonance. We set $\omega_0 = 1470$ cm^{-1}(bend), $\omega_1 = 2890$ cm^{-1}(stretch), and $h_{001} = 30$ cm^{-1}[14]. A necessary condition for Fermi resonance is that $\omega_1 \approx 2\omega_0$, which is met here as $\omega_1/\omega_0 \approx 1.966$. In our model calculations, for the first-order Taylor terms of dipole moment surface μ we set $m_0 = m_1$. The Fermi resonance leads to the extra peak at $\sim$2940 cm^{-1} appearing in Figure 3 of the main text, a peak which is not present in the harmonic approximation.

	# Qubits	$\max\left(\{|a_k|\} \setminus |a_I|\right)$ (Ha)	W (Ha)	$10^{-6}\,W/\epsilon$		
				$\epsilon = 100$ cm^{-1}	$\epsilon = 10$ cm^{-1}	$\epsilon = 1$ cm^{-1}
				455 μHa	45.5 μHa	4.55 μHa
Vibrational	24	0.045	0.146	0.321	3.21	32.1
2-body	36	0.066	0.244	0.536	5.36	53.6
$d = 4$	48	0.088	0.358	0.787	7.87	78.7
Vibrational	24	0.045	0.187	0.411	4.11	41.1
3-body	36	0.066	0.387	0.851	8.51	85.1
$d = 4$	48	0.108	0.695	1.53	15.3	153
Vibrational	24	0.087	0.276	0.607	6.07	60.7
2-body	36	0.126	0.450	0.989	9.89	98.9
$d = 8$	48	0.166	0.651	1.43	14.3	143
Vibrational	24	0.087	0.336	0.738	7.38	73.8
3-body	36	0.126	0.675	1.48	14.8	148
$d = 8$	48	0.192	1.197	2.63	26.3	263
V$_2$ model	24	0.471	2.41	5.30	53.0	530
V$_3$ model	36	0.639	3.35	7.36	73.6	736
V$_4$ model	48	0.752	4.72	10.4	104	1040
Cr$_2$ model	24	0.142	1.70	3.74	37.4	374
Cr$_3$ model	36	0.193	2.41	5.30	53.0	530
Cr$_4$ model	48	0.280	3.08	6.77	67.7	677
Mn$_2$ model	24	0.647	2.75	6.04	60.4	604
Mn$_3$ model	36	0.901	3.79	8.33	83.3	833
Mn$_4$ model	48	1.067	4.74	10.4	104	1040
Fe$_2$ model	24	1.38	5.47	12.0	120	1200
Fe$_3$ model	36	1.84	7.97	17.5	175	1750
Fe$_4$ model	48	1.73	10.1	22.1	221	2210
FeMoco [92]	154	11.8				

TABLE I. Comparing the magnitudes of Hamiltonians. $W = \sqrt{\sum_{k \neq I} a_k^2}$ is related to the Frobenius norm and also relates to the number of measurements required for VQE.